SANDIA REPORT

SAND2000-0217
Unlimited Release
Printed February 2000

Chemical Reactions in TEOS/Ozone Chemical Vapor Deposition

Pauline Ho

Prepared by
Sandia National Laboratories
Albuquerque, New Mexico 87185 and Livermore, California 94550

Sandia is a multiprogram laboratory operated by Sandia Corporation, a Lockheed Martin Company, for the United States Department of Energy under Contract DE-AC04-94AL85000.

Sandia National Laboratories

Issued by Sandia National Laboratories, operated for the United States Department of Energy by Sandia Corporation.

Available to DOE and DOE contractors from
U.S. Department of Energy
Office of Scientific and Technical Information
P.O. Box 62
Oak Ridge, TN 37831

Telephone: (865)576-8401
Facsimile: (865)576-5728
E-Mail: reports@adonis.osti.gov
Online ordering: http://www.doe.gov/bridge

Available to the public from
U.S. Department of Commerce
National Technical Information Service
5285 Port Royal Rd
Springfield, VA 22161

Telephone: (800)553-6847
Facsimile: (703)605-6900
E-Mail: orders@ntis.fedworld.gov
Online order: http://www.ntis.gov/ordering.htm

SAND2000-0217
Unlimited Release
Printed February 2000

Chemical Reactions in TEOS/Ozone Chemical Vapor Deposition

Pauline Ho
Chemical Processing Sciences Department
Sandia National Laboratories
P.O. Box 5800
Albuquerque, NM 87185-0601

Abstract

A reaction mechanism for TEOS/O_3 CVD in a SVG/WJ atmospheric pressure furnace belt reactor has been developed and calibrated with experimental deposition rate data. One-dimensional simulations using this mechanism successfully reproduce the trends observed in a set of 31 experimental runs in a WJ-TEOS999 reactor. Two-dimensional simulations using this mechanism successfully reproduce the average deposition rates for 3 different experimental conditions in a WJ-1500TF reactor, although the deposition profiles predicted by the model are flatter than the experimental static prints.

Acknowledgements

Dr. Vladimir Kudriavtsev* is acknowledged for starting this project, as well as the previous work done for Technical Assistance Agreement 1269, with the support of John Boland. Dr. Kudriavtsev and Dr. Simin Moktari# also performed the two-dimensional calculations that were critical in deciding how to properly compare the lower-dimensional simulations described here with the experimental data. Dr. Jeff Bailey# is thanked for stepping into the management of this project in midstream. Dr. Bailey and Larry Bartholomew# are also thanked for providing experimental data and much insight into the CVD process of interest.

* Present affiliation: CFD Research Corporation, Los Altos, CA

Present affiliation: Silicon Valley Group Thermal Systems, Scotts Valley, CA

I. Introduction

The use of computational models for the design and optimization of chemical vapor deposition (CVD) equipment and processes is becoming increasingly common. Commercial codes for modeling the chemically-reacting flows in such reactors are now available, but chemical reaction mechanisms describing the specific process of interest generally have to be developed for each problem.

This document reports work on the chemistry of TEOS ($Si(OC_2H_5)_4$) and ozone (O_3), which are used to deposit silicon dioxide (SiO_2) films at atmospheric pressure. This work was done under CRADA No. 01512, Task 0.001, the blanket agreement between Sandia National Laboratories (SNL) and SEMI/SEMATECH. It was started with the Semiconductor Equipment Group of Watkins-Johnson (WJ), which has now been acquired by the Silicon Valley Group, Thermal Systems (SVG-TS).

Although the TEOS/O_3 system has been the subject of many investigations, a review of the literature is not included here. Previous work[1] by SNL and WJ showed the limitations of using very simple reaction mechanisms to describe the atmosphere-pressure, moving belt TEOS/O_3 CVD system of interest. The current project was a direct outgrowth of the previous project, and involves the development of a more "fundamentals-based" reaction mechanism. In the past, the computational-fluid dynamics codes being used to model the CVD system of interest were limited in their capabilities to handle chemical reactions, and thus required the use of very simple chemistries. Recent improvements to such codes, however, have significantly increased their capabilities and allow the use of more complex chemical reaction mechanisms.

This document only discusses the development of the chemical reaction mechanism, along with the 0D and 1D simulations used for this purpose. Two-dimensional simulations were done[2] to help calibrate the chemistry. Although they are referred to in this document, they will be described elsewhere.[3]

II. Chemical Reaction Mechanism

The chemical reactions of interest in CVD systems can be subdivided into gas-phase (homogeneous) reactions and gas-surface (heterogeneous) reactions. The knowledge base available in the literature for the former is much greater than for the latter. This is reflected in the size and complexity of the reactions describing the chemistry. For the gas-phase, we have tried to use elementary chemical reactions, with rate parameters either taken from the literature or estimated by analogy with known reactions. In contrast, the surface reaction mechanism is much smaller and contains "lumped" reactions with rate parameters derived by fitting to deposition rate data.

As will be described in more detail below, two variations of our TEOS/O_3 reaction mechanisms are presented here, each with advantages and disadvantages. Version 1 uses simple sticking coefficients to describe the surface reactions, while Version 2 includes the effects of blocking groups on the surface preventing further reaction. The gas-phase chemistry is essentially the same for these two cases.

Developing the reaction mechanism was primarily done with 0D simulations using AURORA[4] and 1D simulations using SPIN.[5] AURORA provides information on sensitivities and rates-of-progress that are valuable in fitting a reaction mechanism to a set of experimental data, but oversimplifies the transport. These codes use CHEMKIN[6] for handling the chemical kinetics part of these reacting flow problems.

A. Gas-Phase Chemistry

The reaction mechanism developed in this work has 20 gas-phase species and 45 gas-phase reactions, although other species and reactions were considered. Table 1 lists the reactions with their corresponding rate parameters, where $k = A\ T^{\beta}\ \exp(-E_a/RT)$. Table 2 gives thermochemical data for the gas-phase and surface species, in the polynomial fit format used by the CHEMKIN[6] software.

The gas-phase reactions in Table 1 are divided into categories. The first category is the decomposition of ozone. It consists of two elementary reactions for ozone decomposition to O_2 taken from the work of Benson and Axworthy,[8] plus two reactions for OH and H atom reactions with O_3 taken from the NIST database.[9] The next category consists of various elementary reactions among H_xO_y species. These are quite well known from combustion and atmospheric chemistry, and were extracted from a hydrocarbon/nitrogen oxidation reaction mechanism by Glarborg.[10]

The other reaction categories involve TEOS and its reaction products, which generally have been less-well studied. Thus, these categories include non-elementary reactions and many rate constants that have been estimated from analogous hydrocarbon reactions. In developing this part of the mechanism, the first step involved obtaining or estimating thermochemical parameters for the species of interest. Then the list of chemically possible reactions was screened by examining the heats of reaction. Exothermic reactions, and reactions with relatively low endothermicities were generally retained.

The category of TEOS reactions with small radicals are primarily hydrogen abstraction reactions, although TEOS hydrolysis is also included. Fortunately, the most important reaction between TEOS and O atoms has been studied experimentally both by Sanago and Zachariah[11] and by Buchta, et al.[7] The kinetic parameters from these two studies are quite close [k = 2.7E12 exp(–2622.8/RT) vs. k = 2.05E13 exp(–2591.0/RT)]. Both were tried in the simulations at various times, but the parameters of Sanago and Zachariah are used in the final mechanism because they gave slightly better fits to the data. Although hydrogen abstraction can occur with different rates at either an α or β position producing different isomers of $C_2H_4OSi(OEt)_3$, these are not tracked separately in this mechanism in the interest of simplicity.

Table 1. Gas-phase reactions for TEOS/O_3 CVD

No.	Reaction	A [a]	β	E_a [b]	Ref.[c]
	Ozone decomposition				
1.	$O_3 + M \leftrightarrow O_2 + O + M$	4.51E15	0.0	24000.0	8
2.	$O + O_3 \leftrightarrow 2O_2$	2.96E13	0.0	6000.0	8
3.	$OH + O_3 \leftrightarrow HO_2 + O_2$	1.15E12	0.0	1987.0	9
4.	$H + O_3 \leftrightarrow OH + O_2$	2.29E11	0.75	0.00	9
	H_2/O_2 Reactions				
5.	$O + OH \leftrightarrow H + O_2$	3.3E11	0.375	-2210.0	10
6.	$O + H_2 \leftrightarrow OH + H$	5.1E04	2.67	6290.0	10
7.	$OH + H_2 \leftrightarrow H_2O + H$	2.1E08	1.52	3450.0	10
8.	$OH + OH \leftrightarrow H_2O + O$	4.3E03	2.70	-2486.0	10
9.	$H + H + M \leftrightarrow H_2 + M$	6.5E17	-1.0	0.0	10
	Third Body:[d] N_2 0.0, O_2 1.5, H_2O 14				
10.	$H + H + N_2 \leftrightarrow H_2 + N_2$	5.4E18	-1.3	0.0	10
11.	$H + O + M \leftrightarrow OH + M$	4.7E18	-1.0	0.0	10
	Third Body:[d] N_2 1.5, O_2 1.5, H_2O 10				
12.	$H + OH + M \leftrightarrow H_2O + M$	8.3E21	-2.0	0.0	10
	Third Body:[d] N_2 2.7, H_2O 17				
13.	$O + O + M \leftrightarrow O_2 + M$	1.9E13	0.0	-1788.0	10
	Third Body:[d] N_2 1.5, O_2 1.5, H_2O 10				
14.	$H + O_2 (+ M) \leftrightarrow HO_2 (+ M)$	4.5E13	0.0	0.0	10
	Low pressure [e]	6.7E19	-1.42	0.0	10
	Third Body:[d] O_2 1.0, H_2 2.3, H_2O 11				
15.	$HO_2 + H \leftrightarrow H_2 + O_2$	4.3E13	0.0	1410.0	10
16.	$HO_2 + H \leftrightarrow OH + OH$	1.7E14	0.0	875.0	10
17.	$HO_2 + H \leftrightarrow O + H_2O$	3.0E13	0.0	1720.0	10
18.	$HO_2 + O \leftrightarrow OH + O_2$	3.2E13	0.0	0.0	10
19.	$HO_2 + OH \leftrightarrow H_2O + O_2$	1.9E16	-1.0	0.0	10

[a] Units depend on reaction order, but are in cm, moles and sec.

[b] Units of cal/mole.

[c] E in this column indicates that the rate parameters were estimated in this work.

[d] Enhanced third body collision efficiencies for the specified molecules.

[e] Rate parameters at low pressure limit for a decomposition/recombination reaction in the pressure-dependent regime.

	TEOS reactions with small radicals				
20.	$Si(OEt)_4 + O \leftrightarrow C_2H_4OSi(OEt)_3 + OH$	2.05E13	0.0	2591.0	11
21.	$Si(OEt)_4 + OH \leftrightarrow C_2H_4OSi(OEt)_3 + H_2O$	1.6E12	0.0	800.0	12 [f,g]
22.	$Si(OEt)_4 + H \leftrightarrow C_2H_4OSi(OEt)_3 + H_2$	2.6E12	0.0	4700.0	12 [f,g]
23.	$Si(OEt)_4 + H_2O \leftrightarrow Si(OEt)_3OH + EtOH$	1.0E11	0.0	25000.0[h]	E
	Reactions of radical intermediates				
24.	$C_2H_4OSi(OEt)_3 + O \leftrightarrow CH_3CHO + OSi(OEt)_3$	3.0E13	0.0	0.0	E
25.	$C_2H_4OSi(OEt)_3 + OH \leftrightarrow CH_3CHO + Si(OEt)_3OH$	3.0E13	0.0	0.0	E
26.	$C_2H_4OSi(OEt)_3 + O_2 \leftrightarrow CH_3COO + Si(OEt)_3OH$	3.0E12	0.0	0.0	E
27.	$C_2H_4OSi(OEt)_3 + O_2 \leftrightarrow CH_3COOH + OSi(OEt)_3$	3.0E12	0.0	0.0	E
28.	$C_2H_4OSi(OEt)_3 + O_3 \leftrightarrow CH_3CHO + OSi(OEt)_3 + O_2$	3.0E13	0.0	0.0	E
29.	$C_2H_4OSi(OEt)_3 + H_2O \rightarrow EtOH + OSi(OEt)_3$	3.0E13	0.0	27000.0	E
30.	$C_2H_4OSi(OEt)_3 \rightarrow C_2H_4 + OSi(OEt)_3$	4.0E14	0.0	39000.0	12 [f]
31.	$C_2H_4OSi(OEt)_3 \leftrightarrow CH_3CHO + Si(OEt)_3$	4.0E14	0.0	47000.0	12 [f]
32.	$OSi(OEt)_3 + Si(OEt)_4 \leftrightarrow C_2H_4OSi(OEt)_3 + Si(OEt)_3OH$	3.0E13	0.0	0.0	E
33.	$OSi(OEt)_3 + O \leftrightarrow O_2 + Si(OEt)_3$	3.0E13	0.0	0.0	E
34.	$OSi(OEt)_3 + H_2O \leftrightarrow OH + Si(OEt)_3OH$	3.0E13	0.0	0.0	E
35.	$Si(OEt)_3 + O_3 \leftrightarrow OSi(OEt)_3 + O_2$	3.0E13	0.0	0.0	E
36.	$Si(OEt)_3 + H_2O \leftrightarrow Si(OEt)_3OH + H$	3.0E13	0.0	0.0	E
37.	$Si(OEt)_3 + Si(OEt)_3OH \leftrightarrow O(Si(OEt)_3)_2 + H$	1.0E12	0.0	0.0	E
38.	$CH_3COO + HO_2 \leftrightarrow CH_3COOH + O_2$	1.0E13	0.0	0.0	E
	Chain termination reactions				
39.	$C_2H_4OSi(OEt)_3 + H \leftrightarrow Si(OEt)_4$	1.0E13	0.0	0.0	E
40.	$OSi(OEt)_3 + H \leftrightarrow Si(OEt)_3OH$	1.0E13	0.0	0.0	E
41.	$Si(OEt)_3 + OH \leftrightarrow Si(OEt)_3OH$	1.0E13	0.0	0.0	E
42.	$Si(OEt)_3 + OSi(OEt)_3 \leftrightarrow O(Si(OEt)_3)_2$	1.0E13	0.0	0.0	E
43.	$CH_3COO + H \leftrightarrow CH_3COOH$	1.0E12	0.0	0.0	E
	Condensation reactions				
44.	$Si(OEt)_3OH + Si(OEt)_4 \leftrightarrow O(Si(OEt)_3)_2 + EtOH$	1.0E11	0.0	15000.0	E
45.	$2\ Si(OEt)_3OH \leftrightarrow O(Si(OEt)_3)_2 + H_2O$	1.0E11	0.0	15000.0	E

[f] Estimated by analogy with TMOS reaction in the referenced paper.

[g] The value used is the TMOS value divided by 10.

[h] This value of Ea used for Version 1. A value of 10000 cal/mole was used for Version 2.

Table 2. Thermochemical Data in CHEMKIN Format

```
Gas-Phase Species:
SI(OET)4          61496H  20C   8O   4SI  1G   300.000  3000.000 1000.00    0 1
 0.14384550E+02 0.91940556E-01-0.48408362E-04 0.12244826E-07-0.12086997E-11    2
-0.16779748E+06-0.26402920E+02 0.36650096E+01 0.11162005E+00-0.42142822E-04    3
-0.16446561E-07 0.12257199E-10-0.16452653E+06 0.31030103E+02                   4
SI(OET)3OH        40894H  16C   6O   4SI  1G   300.000  3000.000 1000.00    0 1
 0.30722271E+02 0.30770605E-01-0.25774402E-05-0.30498899E-08 0.66850084E-12    2
-0.17340573E+06-0.11836710E+03 0.89422655E+01 0.70058122E-01-0.53697897E-06    3
-0.37873331E-07 0.15943972E-10-0.16629886E+06-0.43492889E+00                   4
O                 120186O   1               G  0300.00   5000.00  1000.00     1
 0.02542059E+02-0.02755061E-03-0.03102803E-07 0.04551067E-10-0.04368051E-14    2
 0.02923080E+06 0.04920308E+02 0.02946428E+02-0.16381665E-02 0.02421031E-04    3
-0.16028431E-08 0.03890696E-11 0.02914764E+06 0.02963995E+02                   4
O2                121386O   2               G  0300.00   5000.00  1000.00     1
 0.03697578E+02 0.06135197E-02-0.12588420E-06 0.01775281E-09-0.11364354E-14    2
-0.12339301E+04 0.03189165E+02 0.03212936E+02 0.11274864E-02-0.05756150E-05    3
 0.13138773E-08-0.08768554E-11-0.10052490E+04 0.06034737E+02                   4
O3                1212860   3               G  0300.00   5000.00  1000.00     1
 0.05429371E+02 0.01820380E-01-0.07705607E-05 0.14992929E-09-0.10755629E-13    2
 0.15235267E+05-0.03266386E+02 0.02462608E+02 0.09582781E-01-0.07087359E-04    3
 0.13633683E-08 0.02969647E-11 0.16061522E+05 0.12141870E+02                   4
N2                121286N   2               G  0300.00   5000.00  1000.00     1
 0.02926640E+02 0.14879768E-02-0.05684760E-05 0.10097038E-09-0.06753351E-13    2
-0.09227977E+04 0.05980528E+02 0.03298677E+02 0.14082404E-02-0.03963222E-04    3
 0.05641515E-07-0.02444854E-10-0.10208999E+04 0.03950372E+02                   4
H                 120186H   1               G  0300.00   5000.00  1000.00     1
 0.02500000E+02 0.00000000E+00 0.00000000E+00 0.00000000E+00 0.00000000E+00    2
 0.02547162E+06-0.04601176E+01 0.02500000E+02 0.00000000E+00 0.00000000E+00    3
 0.00000000E+00 0.00000000E+00 0.02547162E+06-0.04601176E+01                   4
H2                121286H   2               G  0300.00   5000.00  1000.00     1
 0.02991423E+02 0.07000644E-02-0.05633828E-06-0.09231578E-10 0.15827519E-14    2
-0.08350340E+04-0.13551101E+01 0.03298124E+02 0.08249441E-02-0.08143015E-05    3
-0.09475434E-09 0.04134872E-11-0.10125209E+04-0.03294094E+02                   4
H2O                20387H   2O   1          G  0300.00   5000.00  1000.00     1
 0.02672145E+02 0.03056293E-01-0.08730260E-05 0.12009964E-09-0.06391618E-13    2
-0.02989921E+06 0.06862817E+02 0.03386842E+02 0.03474982E-01-0.06354696E-04    3
 0.06968581E-07-0.02506588E-10-0.03020811E+06 0.02590232E+02                   4
HO2               BUR95 H   1O   2   00   00G   200.000  6000.000 1000.000    1
 0.41722659E+01 0.18812098E-02-0.34629297E-06 0.19468516E-10 0.17609153E-15    2
 0.61818851E+02 0.29577974E+01 0.43017880E+01-0.47490201E-02 0.21157953E-04    3
-0.24275961E-07 0.92920670E-11 0.29480876E+03 0.37167010E+01 0.15096500E+04    4
C2H4              121286C   2H   4          G  0300.00   5000.00  1000.00     1
 0.03528418E+02 0.11485185E-01-0.04418385E-04 0.07844600E-08-0.05266848E-12    2
 0.04428288E+05 0.02230389E+02-0.08614880E+01 0.02796162E+00-0.03388677E-03    3
 0.02785152E-06-0.09737879E-10 0.05573046E+05 0.02421148E+03                   4
CH3CHO            120186C   2O   1H   4     G  0300.00   5000.00  1000.00     1
 0.05868650E+02 0.10794241E-01-0.03645530E-04 0.05412912E-08-0.02896844E-12    2
-0.02264568E+06-0.06012946E+02 0.02505695E+02 0.13369907E-01 0.04671953E-04    3
-0.11281401E-07 0.04263566E-10-0.02124588E+06 0.13350887E+02                   4
ETOH               71091C   2H   6O   1     G  0300.00   5000.00  1000.00     1
 0.79087286E+01 0.12227729E-01-0.35144249E-05 0.42572035E-09-0.15468177E-13    2
-0.31943867E+05-0.16426895E+02 0.16487226E+01 0.21139644E-01 0.32672033E-05    3
-0.16375399E-07 0.73521788E-11-0.29673598E+05 0.18271423E+02                   4
ETO                70998H   5C   2O   1    0G   300.000  3000.000 1000.00     1
 0.29337879E+01 0.21304490E-01-0.10803929E-04 0.26500268E-08-0.25512631E-12    2
-0.20779635E+04 0.10162778E+02 0.14075698E+01 0.25049131E-01-0.12933056E-04    3
 0.17792313E-08 0.52637367E-12-0.16529579E+04 0.18120332E+02                   4
CH3COO             70798H   3C   2O   2    0G  0300.00   3000.00  1000.00     1
```

```
 0.32609145E+01 0.18283757E-01-0.96171090E-05 0.24287846E-08-0.23929524E-12    2
-0.23659970E+05 0.12650950E+02 0.19962463E+01 0.19593159E-01-0.64440015E-05    3
-0.27869632E-08 0.17586114E-11-0.23203349E+05 0.19730119E+02                   4
CH3COOH            71398H   4C   2O   2    0G   300.000  4000.00  1000.00     1
 0.51094633E+01 0.17736435E-01-0.82137494E-05 0.17593858E-08-0.14319261E-12    2
-0.54870495E+05 0.32785188E+00 0.42050999E+00 0.31807685E-01-0.26342195E-04    3
 0.14558339E-07-0.41959973E-11-0.53563529E+05 0.24457850E+02                   4
!  The following are estimated thermochemical data
O(SI(OET)3)2       011196O   7SI  2C  12H  30G   298.15   3000.00  1000.00     1
 2.37118816E+01 1.38595819E-01-7.21792312E-05 1.81146351E-08-1.77790129E-12    2
-2.97149250E+05-6.43604507E+01 1.70925987E+00 1.97589725E-01-1.16528972E-04    3
 1.78428774E-08 5.85231559E-12-2.91318375E+05 4.89922791E+01                   4
OSI(OET)3          032798SI  1O   4C   6H  15G   298.15   3000.00  1000.00     1
 1.12083378E+01 7.70037100E-02-4.02504957E-05 1.01245767E-08-9.95064599E-13    2
-1.30548180E+05-1.95242100E+01 6.21738625E+00 7.91375637E-02-1.60659947E-05    3
-2.46821941E-08 1.24843165E-11-1.28679836E+05 8.95836926E+00                   4
C2H4OSI(OET)3      032798SI  1O   4C   8H  19G   298.15   3000.00  1000.00     1
 1.18439360E+01 9.77492258E-02-5.11394210E-05 1.28724391E-08-1.26581005E-12    2
-1.44889656E+05-2.19231243E+01 5.08996964E+00 1.02091007E-01-2.28924528E-05    3
-2.96310336E-08 1.54028682E-11-1.42430078E+05 1.62670174E+01                   4
SI(OET)3           032898SI  1O   3C   6H  15G   298.15   3000.00  1000.00     1
 8.46764469E+00 7.67193064E-02-4.01140351E-05 1.00932791E-08-9.92274405E-13    2
-9.98335234E+04-5.87761784E+00 5.00523376E+00 7.18663335E-02-3.55981024E-06    3
-3.46066216E-08 1.54687825E-11-9.82465938E+04 1.54004326E+01                   4
Surface Species:
SIG3(OH)           121591O   2SI  1H   1     I    300.00   3000.00 1000.00     1
 0.66466584E+01 0.33231564E-02-0.29541198E-06-0.31399386E-09 0.69825405E-13    2
-0.98982922E+05-0.33869411E+02 0.26748490E+01 0.12014943E-01-0.13939117E-05    3
-0.83051193E-08 0.44394740E-11-0.97866992E+05-0.13004364E+02                   4
SIGE3               62692C   6H  15O   3SI  1I    300.00   3000.00 1000.00     1
 0.25609777E+02 0.30346680E-01-0.24455890E-05-0.30030116E-08 0.65423480E-12    2
-0.13233747E+06-0.11858306E+03 0.72320976E+01 0.60353167E-01 0.21851304E-05    3
-0.28773197E-07 0.10164894E-10-0.12596620E+06-0.17743988E+02                   4
SIO2(D)            J 3/67SI  1O   2          S   300.000  1685.000             1
 0.24753989E 01 0.88112187E-03-0.20939481E-06 0.42757187E-11 0.16006564E-13    2
-0.81255620E 03-0.12188747E 02 0.84197538E 00 0.83710416E-02-0.13077030E-04    3
 0.97593603E-08-0.27279380E-11-0.52486288E 03-0.45272678E 01                   4
```

The next category, reactions among radical intermediates, primarily includes bimolecular reactions that interconvert the various Si-O-H-C species. These reactions provide a chain mechanism by which one oxygen atom (from an ozone molecule) can potentially convert multiple TEOS molecules into more-reactive intermediate species. For many of these reactions, the reactants are appropriate for an elementary reaction, but the products given represent molecular rearrangements that probably occur in multiple steps. Endothermic reactions were given activation energies on the order of the endothermicity. Relatively high A factors were generally used, with radical-radical reactions being faster than radical-molecule reactions. Although they turn out to be unimportant, two reactions involving the unimolecular decay of

$C_2H_4OSi(OEt)_3$ are included. These molecules are sufficiently large that they should be at the high pressure limit at 1 atm, so pressure-dependent fall-off parameters were not determined.

The next category, chain termination reactions, are radical recombination reactions that can interrupt the radical chain reactions that decompose the TEOS. Again, these molecules are assumed to be big enough to be in their high-pressure limits at 1 atm pressures, so explicit fall-off parameters are not provided. For reaction 43, the molecules involved are smaller, so a smaller A factor was used, although this reaction also turns out not to be very important.

The two reactions in the last category, condensation reactions, represent the formation of hexaethoxydisiloxane. This can be thought of as TEOS dimerization, which could be the first step in forming larger polymeric liquid/solid species. The formation of these solid byproducts are a significant concern in TEOS/O_3 CVD. The present simulations, however, suggest that gas-phase formation of dimers is not significant in the main reaction zone. This in turn suggests that direct gas-phase polymerization is not likely to be the major source of these byproducts, but rather condensation and polymerization on surfaces (TEOS is commonly used in the condensed phase for the production of silicon oxide sols and gels). Note that this study did not focus on the parts of the reactor downstream from the deposition zone, where reactions not considered here may occur. Also, if there turned out to be significant errors in the thermochemical and kinetic data used, this would also affect this conclusion.

B. Surface Chemistry

The surface reaction mechanisms shown in Table 3 for Version 1 and Table 4 for Version 2 are much smaller than the gas-phase mechanism shown in Table 1. The surface reactions are also "lumped" rather than elementary chemical reactions. As mentioned above, this is primarily a result of the smaller knowledge base in the literature for surface reactions. Although many of the trends observed in the deposition rate data could be reproduced using Version 1, which has no specified surface species (non-site-specific sticking coefficients), the dependence on TEOS mole fraction (flow rate) was too strong, so Version 2, which accounts for surface site-blocking, was developed.

Table 3. Version 1 Surface Reactions for TEOS/O_3 CVD

No.	Reaction	A	E_a	Notes*
1.	$Si(OEt)_3OH \rightarrow H_2O + 2\ C_2H_4 + EtOH + SiO_2(D)$	5.0E-8	-10000.0	Stick, Fit
2.	$OSi(OEt)_3 \rightarrow O_2 + 1.5H_2 + 3\ C_2H_4 + SiO_2(D)$	6.0E-7	-10000.0	Stick, Estd
3.	$Si(OEt)_3 \rightarrow H_2O + 3\ C_2H_4 + 0.5\ H_2 + SiO_2(D)$	6.0E-7	-10000.0	Stick, Estd
4.	$C_2H_4OSi(OEt)_3 \rightarrow O_2 + 1.5\ H_2 + 4\ C_2H_4 + SiO_2(D)$	6.0E-7	-10000.0	Stick, Estd
5.	$O \rightarrow 0.5\ O_2$	1.0	0.0	Stick, Estd
6.	$OH \rightarrow 0.5\ H_2 + 0.5\ O_2$	1.0	0.0	Stick, Estd
7.	$H \rightarrow 0.5\ H_2$	1.0	0.0	Stick, Estd

Table 4. Version 2 Surface Reactions for TEOS/O_3 CVD

No.	Reaction	A	E_a	Notes*
1.	$Si(OEt)_3OH + SiG_3OH(s) \rightarrow H_2O + SiGE_3(s) + SiO_2(D)$	1.8E-9	-15000.0	Stick, Fit
2.	$SiGE_3(s) \rightarrow 2\ C_2H_4 + EtOH + SiG_3OH(s)$	12.0	0.0	Fit
3.	$OSi(OEt)_3 + SiG_3OH(s) \rightarrow 0.5O_2 + 0.5H_2 + SiGE_3(s) + SiO_2(D)$	5.0E-8	-15000.0	Stick, Estd
4.	$Si(OEt)_3 + SiG_3OH(s) \rightarrow 0.5\ H_2 + SiGE_3(s) + SiO_2(D)$	5.0E-8	-15000.0	Stick, Estd
5.	$C_2H_4OSi(OEt)_3 + SiG_3OH(s) \rightarrow CH_3CHO + 0.5\ H_2 + SiGE_3(s) + SiO_2(D)$	5.0E-8	-15000.0	Stick, Estd
6.	$O \rightarrow 0.5\ O_2$	1.0	0.0	Stick, Estd
7.	$OH \rightarrow 0.5\ H_2 + 0.5\ O_2$	1.0	0.0	Stick, Estd
8.	$H \rightarrow 0.5\ H_2$	1.0	0.0	Stick, Estd

* "Stick" indicates that the reaction parameters given are for a sticking coefficient. "Fit" indicates that the rate parameters were determined by fitting to deposition rate data. "Estd" indicates that rate parameters were estimated.

There are a variety of possible surface species in this system, namely a silicon atom with any combination (adding up to 4) of: 1) Si-O-Si bonds to the bulk SiO_2, 2) a bond to an ethoxy group, 3) a bond to a fragment of an ethoxy group (missing one or more H or C atoms), 4) a fragment of an ethoxy group with added O atoms or OH groups, 5) dangling bonds, 6) a bond to an O atom that has a dangling bond, 7) a bond to a hydroxyl group (OH), or 8) bond to a H atom. In addition to these simple one-site surface species, silicon oxide surfaces are also known to have groups such as "coordinated OH pairs" in which the bonding and reactivity at one Si atom is affected by the presence/absence of functional groups on an adjacent silicon atom. In this work, however, most of these details are neglected in the interest of simplicity and restricted resources.

Although it is now possible to treat multiple surface species in the codes used for the higher-order simulations, the computational complexity of such problems still require a minimum of species and reactions, and the factorial nature of the problem makes it unrealistic to include a large number of surface species.

In Version 1 of the mechanism, no surface species are specified, while Version 2 includes only two surface species: $SiG_3OH(s)$, representing silicon with three bonds to the glass bulk and one reactive OH group, and $SiGE_3(s)$ representing a silicon with one bond to the bulk and three ethoxy groups. The thermochemical data for surface species provided in Table 2 were taken from previous work on TEOS.[13] They are needed to satisfy error-checking routines in the software, but are not really used in the calculations because all the surface reactions are written as irreversible reactions. A surface site density of 1.168×10^{-9} moles cm^{-2} and a bulk density for SiO_2 of 2.33 g cm^{-3} are used.

The first surface reaction in both versions of the mechanism is the adsorption of $Si(OEt)_3OH$ from the gas with on the surface. The rate parameters correspond to sticking coefficients of $\sim3\times10^{-5}$ at 500°C, which are reasonable but on the low side. This reaction was given a negative activation energy in order to reproduce the observed decrease in deposition rate with increasing temperature. Negative activation energies for these kinds of surface reactions generally result from a competition between desorption and reaction, following an adsorption step, which have been combined into one step here.

Version 1 "lumps" all of the surface steps of adsorption, intermediate reactions to eliminate gas-phase byproducts, and deposition of the oxide into one single step. In Version 2, the process of $Si(OEt)_3OH$ adsorption on $SiG_3OH(s)$ open sites is "lumped" with the reaction to eliminate water and form $SiGE_3(s)$ while "depositing" the Si atom that was originally on the surface into the bulk, as it now has 4 Si-O-Si bonds. Version 2 treats the decomposition of $SiGE_3(s)$ groups, releasing ethylene and ethanol to the gas-phase and regenerating $SiG_3OH(s)$ as a separate reaction (reaction 2 in Table 4). Although written as a single reaction, this undoubtedly occurs in multiple steps, probably involving the attack of radical species from the gas-phase. However, in

the interest of simplicity, this is written as a single step with rate parameter determined by fitting to the deposition rate data.

The next three surface reactions are the adsorption/reaction of $OSi(OEt)_3$, $Si(OEt)_3$, and $C_2H_4OSi(OEt)_3$, which are three radical species formed by decomposition of TEOS. These are analogous to the first surface reaction for $Si(OEt)_3OH$, and have been given the same negative activation energies. Larger A factors are used because these species should be somewhat more reactive than $Si(OEt)_3OH$ due to their radical nature. However, the simulations indicate that these species are present in such low concentration that these reactions are not very important in determining deposition rates.

The last three reactions represent the loss of O atoms, OH radicals, and H atoms at the surface. Although these reactions are written as producing O_2 and H_2, the reality is much more complex, involving a variety of abstraction, adsorption and elimination reactions that are all being swept under the carpet. These reactions are written without specifying a surface species, which indicates that they occur on all sites uniformly. These radicals are expected to be highly reactive and have been given reaction probabilities of unity. Calculated rates-of-progress in the 0D simulations indicate that these surface recombination reactions represent the primary loss channels for O atoms and OH radicals, as well as a substantial loss channel for H atoms, for the CVD conditions explored in this work.

III. Comparisons to Experimental Data

The reaction mechanisms developed here were fit to a matrix of 31 deposition rate experiments done at WJ in 1990. This data set was taken with an older reactor geometry (WJ-TEOS999), but it was chosen for this study because it covers a much wider range of temperatures and gas flow ratios than most newer data sets. Table 5 lists the experimental conditions and deposition rates.

The data in this table represent experiments in which a wafer moves under a static injector. Obtaining deposition rates from these "dynamic" experiments requires correcting for the speed of the wafer movement and the number of passes. The numbers in the table average the deposition over a 1.8 inch zone that roughly corresponds to the width of the injector. However, static wafer experiments quite clearly show that the deposition occurs over a wider zone and is far from a 1.8" wide top hat profile. This assumption of a 1.8" wide deposition zone introduces an arbitrary scaling factor into the experimental data which, in turn, introduces some uncertainty in how to correctly compare them with the simulations. The eventual goal of this work is to be able to simulate deposition rates for either static or moving wafer experiments. So the apparently-straightforward approach of matching the deposition rates from the 0D or 1D simulations to the dynamic deposition rates in Table 5 is not the correct thing to do.

The dimensionality of the simulations definitely affect the predicted deposition rates. Depending on the details of the mechanism, the deposition rates from the 0D simulations ranged from several times higher than, to somewhat lower than, the deposition rates from the 1D simulations. Figure 1 shows a comparison of 0D and 1D simulations for the combination of the gas-phase mechanism in Table 1 and the surface mechanism in Table 3. The results are plotted in the order listed in Table 5, which is roughly in order of increasing temperature. For this version of the reaction mechanism, the 0D results are significantly higher than the 1D results, especially at the lower temperatures.

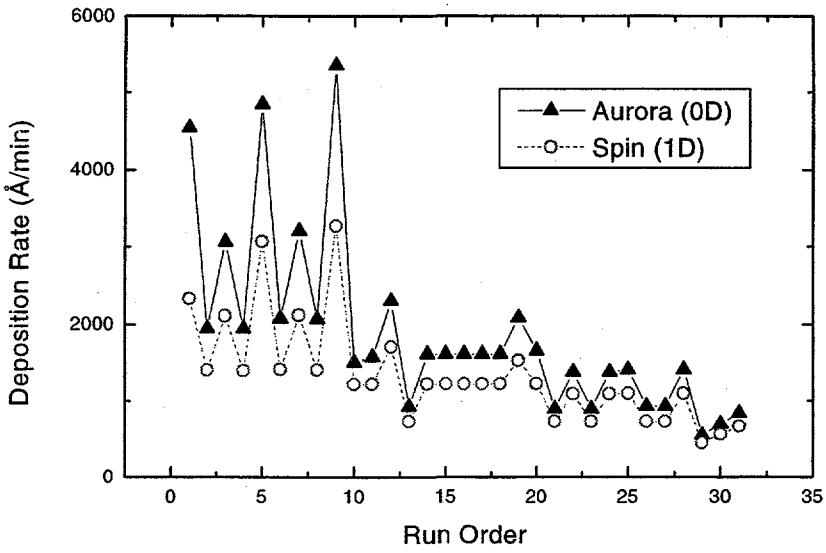

Figure 1. Comparison Between 0D and 1D Simulations using Version 1.

As a result of this sensitivity to dimensionality, a combination of 2D simulations (done using CFD-ACE$^{+CHEMKIN}$,[14] to be described elsewhere[3]) and experimental data in a newer reactor geometry (WJ-1500TF) where both dynamic and static print data were available, were used to calibrate the deposition rates in the reaction mechanisms. Profiles from a 2D simulation were converted to an effective "1.8 inch average" by numerical integration, which could then be compared with the corresponding experimental values. This also reduced the effect of the profile shapes, which were significantly flatter in the simulations than in the experiments. Although static profile shapes are known to change with experimental conditions, unfortunately no information on static profile shapes are available for the experimental data set in Table 5.

Figure 2 shows a comparison between the 1D simulations using Version 1 and the experimental deposition rates. The model successfully reproduces the general trends observed in the data, and have been scaled to give the correct magnitude for the deposition rate. There are cases where model and experiment do not agree well, but some of these may be indicative of other difficulties. For example, the 8th and 9th points in the figure show a decreasing experimental deposition rate as the TEOS mole fraction was increased, which is the opposite of all other such cases as well as the model results. These simulations also exhibit larger variations between some

of the runs than experiment, i.e. the 3rd and 4th points. The differences between these sets of experimental conditions appear primarily to be differences in the TEOS concentration. Version 2 of the mechanism, which includes the kinetic effects of surface coverage by blocking groups, was developed in an effort to decrease the size of these variations in the model predictions.

Figure 3 shows a comparison between the 1D simulations using Version 2 and the experimental deposition rates. The addition of surface-site specific chemistry does reduce the strength of the dependence on TEOS concentration. This version of the mechanism thus does a better job of capturing the trends exhibited in this set of experimental data. Note that a somewhat higher scaling factor has been used to match the magnitude of the model predictions to the experimental data. However, in 2D simulations, Version 2 of the mechanism gave flatter deposition profiles than Version 1, and both were flatter than experimentally observed. Thus it was decided that Version 1 gave better overall agreement with the data currently available.

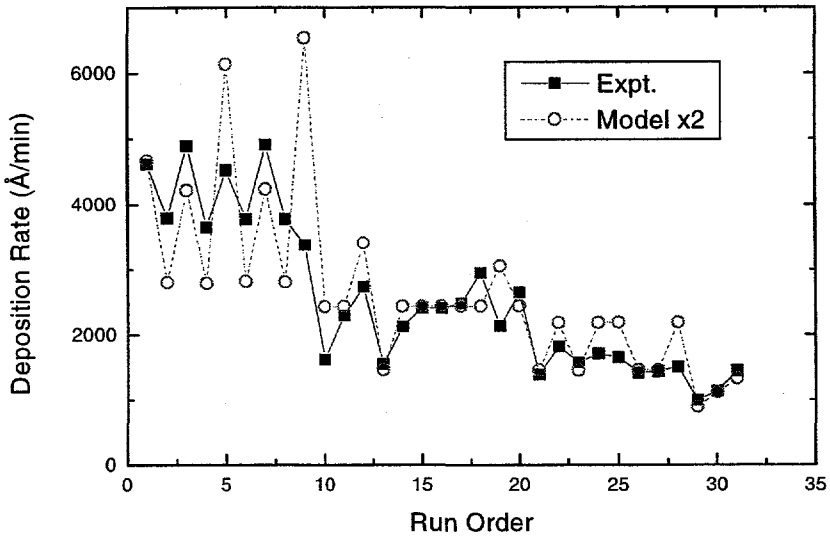

Figure 2. Comparison between experimental deposition rates and 1D simulations using Version 1.

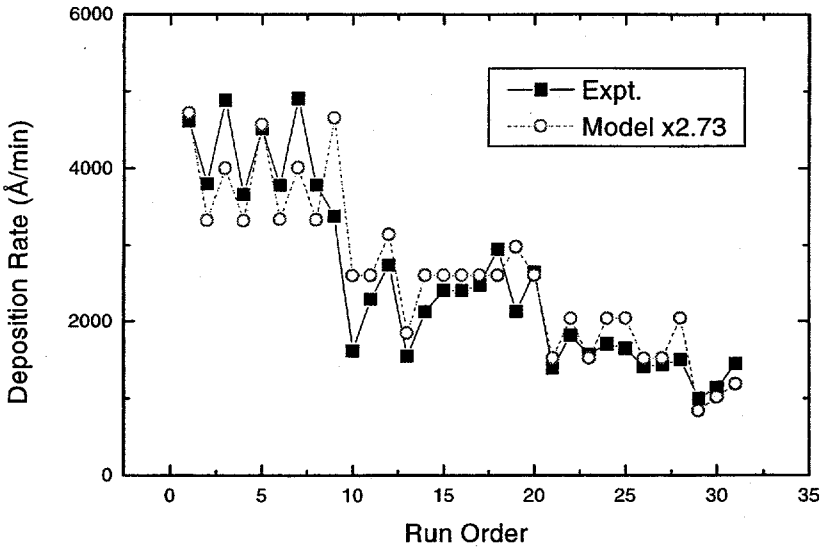

Figure 3. Comparison between experimental deposition rates and 1D simulations using Version 2.

Table 5. Experimental Conditions and Deposition Rate Data.

Run #	Temp (°C)	Dep Rate (Å/min)	TEOS (sccm)	N_2 (slm)	O_2 (slm)	O_3 (slm)	TEOS mole fr.	N_2 mole fr.	O_2 mole fr.	O_3 mole fr.
1059	305	4615	25	21.9563	3.8813	0.1625	0.0010	0.8437	0.1491	0.0062
1043	365	3796	20	19.7500	2.1500	0.1000	0.0009	0.8969	0.0976	0.0045
1047	365	4888	30	18.6250	3.2250	0.1500	0.0014	0.8454	0.1464	0.0068
1045	365	3658	20	17.7500	4.1500	0.1000	0.0009	0.8061	0.1885	0.0045
1049	365	4517	30	7.6250	6.2250	0.1500	0.0021	0.5435	0.4437	0.0107
1044	365	3781	20	19.7800	2.0600	0.1600	0.0009	0.8983	0.0936	0.0073
1048	365	4909	30	18.6700	3.0900	0.2400	0.0014	0.8475	0.1403	0.0109
1046	365	3781	20	17.7800	4.0600	0.1600	0.0009	0.8074	0.1844	0.0073
1050	365	3383	30	6.6700	6.0900	0.2400	0.0023	0.5119	0.4674	0.0184
1027	425	1621	25	13.9188	3.9938	0.0875	0.0014	0.7722	0.2216	0.0049
1025	425	2297	25	16.4375	1.4375	0.1250	0.0014	0.9119	0.0798	0.0069
1064	425	2740	35	14.0888	3.6838	0.2275	0.0019	0.7812	0.2043	0.0126
1031	425	1546	15	15.5738	2.3288	0.0975	0.0008	0.8645	0.1293	0.0054
1030	425	2127	25	13.9563	3.8813	0.1625	0.0014	0.7743	0.2153	0.0090
1028	425	2414	25	13.9563	3.8813	0.1625	0.0014	0.7743	0.2153	0.0090
1026	425	2412	25	13.9563	3.8813	0.1625	0.0014	0.7743	0.2153	0.0090
1032	425	2485	25	13.9563	3.8813	0.1625	0.0014	0.7743	0.2153	0.0090
1033	425	2949	25	13.9563	3.8813	0.1625	0.0014	0.7743	0.2153	0.0090
1062	425	2129	25	7.4563	6.3813	0.1625	0.0018	0.5316	0.4550	0.0116
1063	425	2647	25	13.9938	3.7688	0.2375	0.0014	0.7764	0.2091	0.0132
1013	485	1387	20	11.7500	2.1500	0.1000	0.0014	0.8381	0.1534	0.0071
1009	485	1817	30	10.6250	3.2250	0.1500	0.0021	0.7573	0.2299	0.0107
1010	485	1568	20	9.7500	4.1500	0.1000	0.0014	0.6954	0.2960	0.0071
1014	485	1706	30	7.6250	6.2250	0.1500	0.0021	0.5435	0.4437	0.0107
1012	485	1647	30	10.6610	3.1170	0.2220	0.0021	0.7599	0.2222	0.0158
1008	485	1410	20	11.7800	2.0600	0.1600	0.0014	0.8402	0.1469	0.0114
1011	485	1433	20	9.7800	4.0600	0.1600	0.0014	0.6976	0.2896	0.0114
1015	485	1501	30	6.1700	7.5900	0.2400	0.0021	0.4398	0.5410	0.0171
1001	545	995	20	10.7650	3.1050	0.1300	0.0014	0.7678	0.2215	0.0093
1000	545	1133	25	9.9563	3.8813	0.1625	0.0018	0.7099	0.2767	0.0116
1006	545	1445	30	9.1475	4.6575	0.1950	0.0021	0.6520	0.3320	0.0139

IV. Mechanism Reduction for Higher Dimension Simulations

The reaction mechanism presented above was developed to be based on fundamental chemical kinetic data available from the literature, and to be fairly complete. This means that some of the species and reactions, while known, may not be important during TEOS/O_3 CVD. For the 0D and 1D simulations, the presence of such reactions is not an issue, as these codes run in seconds-to-minutes. For higher-dimensional simulations, however, it is important to reduce the size of the reaction set in order to get solutions in a reasonable amount of time.

For two-dimensional simulations, the reaction mechanisms had to be reduced to no more than 17 gas-phase species. This was done by dropping $Si(OEt)_3$, $O(Si(OEt)_3)_2$, and CH_3CHO, along with their reactions. The sensitivity and rate-of-progress features of the 0D simulations were used to choose which species could be eliminated. 1D simulations using the reduced reactions gave nearly identical results to the full reaction mechanism results shown in either Figure 2 or Figure 3, confirming the validity of the mechanism reduction.

For planned three-dimensional simulations, it is even more important to reduce the chemistry set to the bare minimum, in terms of both number of species and number of reactions. This was done for Version 1, using the procedure outlined above, but applying it more aggressively. This led to a very reduced reaction mechanism was obtained that consists of reactions 1, 20, 26, 27 and 32 from Table 1, and reactions 1, 5 and 6 from Table 3. Zero D simulations using this set of reactions gave results within 4% of the full Version 1 results shown in Figure 1. One D simulations for the three experimental conditions in the WJ-1500TF reactor gave results within 2% of the full Version 1 simulations.

Caution should be used with this reduced reaction set. If experimental conditions become of interest that differ significantly from those tested here, it would be best to go back to the larger mechanism and repeat the reduction process. This small mechanism was also produced by examining effects on deposition rate only. Thus, it should not be used to look at questions of gas-phase byproduct distribution, or to study regions far from the deposition zone.

V. Conclusions

Two versions of a reaction mechanism for TEOS/O_3 CVD in a SVG/WJ furnace belt reactor have been developed and calibrated with experimental deposition rate data. One-dimensional simulations using this mechanism successfully reproduce the trends observed in a set of 31 experimental runs in a WJ-TEOS999 reactor. Two-dimensional simulations using this mechanism successfully reproduce the average deposition rates for 3 different experimental conditions in a WJ-1500TF reactor, although the shapes of the deposition profiles predicted by the model are flatter than the experimental static prints.

Simulations using this reaction mechanism give deposition rates that are much closer to the experimental observations than the mechanisms used in previous studies of this system. This is partially a result of greater completeness and complexity of the mechanism, and partially a result of the calibration process. A test of the mechanism would be to use it in simulations of other TEOS/O_3 CVD systems, perhaps using data in the literature, but this did not fall within the scope of this project.

In the course of this work, a number of questions arose as to the best way to compare the results of the simulations with the experimental data. These primarily dealt with 1) how to transfer between "dynamic" deposition rate measurements and "static prints", and 2) how to calibrate the magnitudes of the deposition rates across simulations of different dimensionality. This reaction mechanism, like all chemical reaction mechanisms, is still imperfect and incomplete. But it should prove useful in studies of possible equipment and process alterations, if the conditions do not differ radically from those used to develop the models. In addition to uncertainties in the chemistry part of these models, there may also be significant uncertainties in some of the boundary conditions (surface temperatures or gas velocities) and/or transport properties.

VI. References

1. P. Ho, J. Johannes, and V. Kudriavtsev, "Report of Work Done for Technical Assistance Agreement 1269 Between Sandia National Laboratories and the Watkins-Johnson Company: Chemical Reactions Mechanisms for Computational Models of SiO_2 CVD", Sandia National Laboratories Report No. SAND97-2328, Oct. 1997.
2. Vladimir Kudriavstev and Simin Moktari, private communication.
3. J. Bailey, V. V. Kudriavstev, S. Moktari, and P. Ho, in preparation.
4. E. Meeks, H. K. Moffat, J. F. Grcar, and R. J. Kee, "AURORA: A Fortran Program for Modeling Well Stirred Plasma and Thermal Reactors with Gas and Surface Reactions", Sandia National Laboratories Report, SAND96-8218 (1996).
5. M. E. Coltrin, R. J. Kee, G. H. Evans, E. Meeks, F. M. Rupley, and J. F. Grcar, "SPIN: A Fortran Program for Modeling One-Dimensional Rotating-Disk / Stagnation-Flow Chemical Vapor Deposition Reactors", Sandia National Laboratories Report, SAND91-8003 (1991).
6. R. J. Kee, F. M. Rupley, J. A. Miller, M. E. Coltrin, J. F. Grcar, E. Meeks, H. K. Moffat, A. E. Lutz, G. Dixon-Lewis, M. D. Smooke, J. Warnatz, G. H. Evans, R. S. Larson, R. E. Mitchell, L. R. Petzold, W. C. Reynolds, M. Caracotsios, W. E. Stewart, and P. Glarborg, , "Chemkin Collection, vers. 3.02", Reaction Design, Inc., (1997).
7. C. Buchta, H. Gg. Wagner and W. Wittchow, *Z. Phys. Chem.*, **190**, 167 (1995)
8. S. W. Benson and A. E. Axworthy, Jr., *J. Chem. Phys.*, **26**, 1718 (1957).
9. F. Westley, D. H. Frizzell, J. T. Herron, R. F. Hampson, and W. G. Mallard, NIST Standard Reference Database 17: NIST Chemical Kinetics Database, U. S. Department of Commerce, (Gaithersburg, MD, 1993).
10. P. Glarborg, "Hydrocarbon/Nitrogen Oxidation Mechanism, version 2.03", on CHEMKIN website (www.ran.sandia.gov/chemkin/mechanisms/JAMiller/pgmech), 1996.
11. O. Sanago and M. R. Zachariah, *J. Electrochem. Soc,* **144,** 2919 (1997).
12. J. C. S. Chu, R. Soller, M. C. Lin, and C. F. Melius, *J. Phys. Chem.,* **99,** 663 (1995) .

13. Michael E. Coltrin, Pauline Ho, Harry K. Moffat and Richard J. Buss, "Chemical Kinetics in Chemical Vapor Deposition: Growth of Silicon Dioxide from Tetraethoxysilane (TEOS)", Thin Solid Films, accepted.
14. Available from CFD Research Corporation, 215 Wynn Drive, Huntsville, Alabama 35805, http://www.cfdrc.com.

Initial Distribution:
Unlimited Release

1 Richard Savage, Ph.D.
Silicon Valley Group Thermal Systems
440 Kings Village Rd.
Scotts Valley, CA 95066

1 Larry Bartholomew
Silicon Valley Group Thermal Systems
440 Kings Village Rd.
Scotts Valley, CA 95066

5 Jeff Bailey, Ph.D.
Silicon Valley Group Thermal Systems
440 Kings Village Rd.
Scotts Valley, CA 95066

1 Simin Mokhtari, Ph.D. c/o
Silicon Valley Group Thermal Systems
440 Kings Village Rd.
Scotts Valley, CA 95066

1 Dr. Vladimir Kudriavtsev
CFDRC West Coast Branch
4962 El Camino Real, Suite 221
Los Altos, CA 94022

1 Mr. Fritz Owens
CFD Research Corporation
Cummings Research Park
215 Wynn Drive
Huntsville, AL 35805

1 Dr. Sura Kim
CFD Research Corporation
Cummings Research Park
215 Wynn Drive
Huntsville, AL 35805

1 Dr. Ashok Singhal
CFD Research Corporation
Cummings Research Park
215 Wynn Drive
Huntsville, AL 35805

1 Dr. Sam Lowry
CFD Research Corporation
Cummings Research Park
215 Wynn Drive
Huntsville, AL 35805

1 Prof. John E. Crowell
Department of Chemistry,
University of California, San Diego
La Jolla, CA 92093-0314

1 Dr. Erik Egan
Reaction Design
6440 Lusk Blvd. Suite D209
San Diego, CA 92121

1 Dr. Ellen Meeks
Reaction Design
6440 Lusk Blvd. Suite D209
San Diego, CA 92121

	MS	
15	0601	P. Ho, 01126
1	0601	J. Y. Tsao, 01126
1	0834	J. Johannes, 09114
1	1077	L. M. Cecchi, 01722
1	1427	S. T. Picraux, 01100
1	9018	Central Technical Files, 08940-2
2	0899	Technical Library, 04916
1	0612	Review & Approval Desk, 04912 For DOE/OSTI
1	1380	Technology Transfer, 04331